Title

THE INFLUENCE OF MICROSTRUCTURE ON THE PROPERTIES OF BRONZE-PROCESSED MULTIFILAMENTARY WIRE

Author

Wu, I.W.

Publication Date

1983-05-01

Lawrence Berkeley Laboratory
UNIVERSITY OF CALIFORNIA

Materials & Molecular
Research Division

Presented at the United States-Japan Workshop on
High Field Superconducting Materials for Fusion,
San Diego, CA, May 23-25, 1983

THE INFLUENCE OF MICROSTRUCTURE ON THE PROPERTIES OF BRONZE-PROCESSED MULTIFILAMENTARY WIRE

I.W. Wu, D.R. Dietderich, W.V. Hassenzahl,
and J.W. Morris, Jr.

May 1983

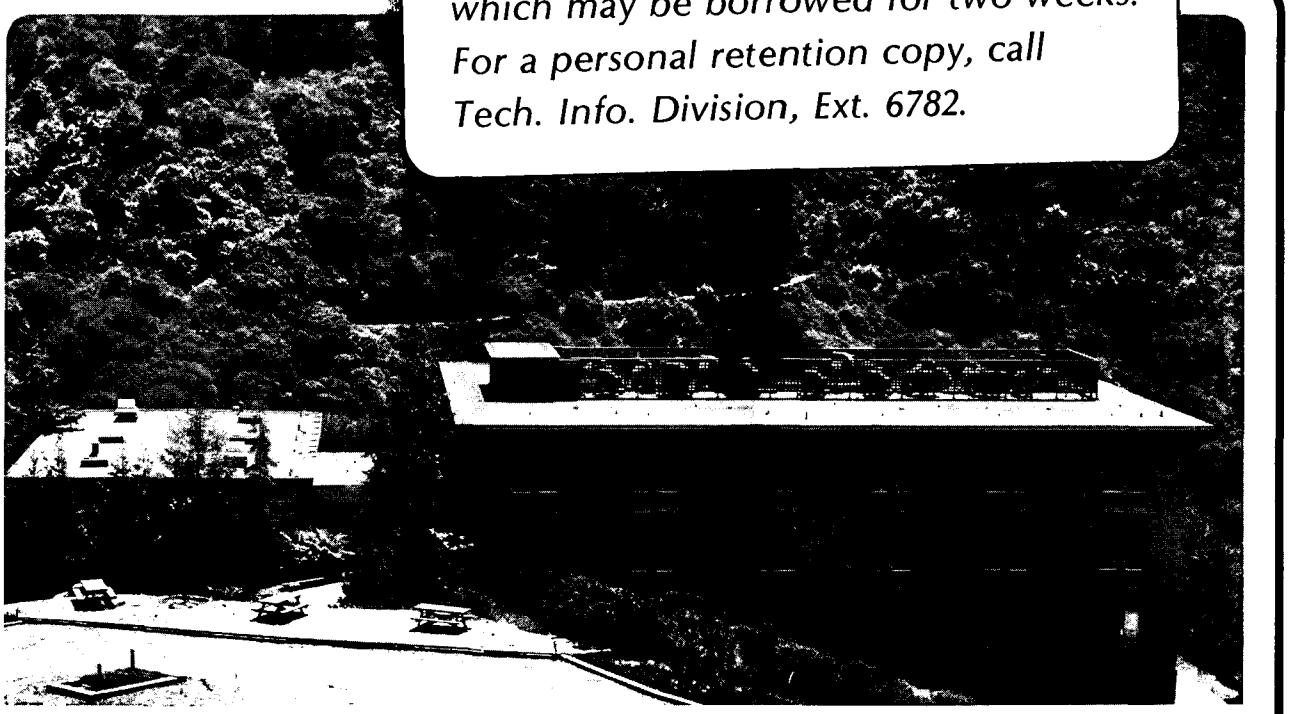

Prepared for the U.S. Department of Energy under Contract DE-AC03-76SF00098

DISCLAIMER

THE INFLUENCE OF MICROSTRUCTURE ON THE PROPERTIES OF BRONZE-PROCESSED MULTIFILAMENTARY WIRE

I.W. Wu, D.R. Dietderich, W.V. Hassenzahl, and J.W. Morris, Jr.

Dept. of Materials Science and Mineral Engineering, Univ. of California, and Lawence Berkeley Laboratory, Berkeley, California 94720

SUMMARY

The A15 layer of a commercial Airco wire containing 2869 Nb filaments was analyzed as a function of heat treatment. Its microstructure is composed of three morphologically distinct concentric shells. The central shell consists of fine equiaxed grains and has a nearly stoichiometric Sn concentration. High resolution electron microscopic analysis suggests that the fine grains are formed through the polygonization of dislocations. The homogeneous composition through the fine-grained layer is a probable consequence of the small grain size, which permits relatively rapid chemical redistributions through grain boundary diffusion. In contrast, the chemical gradient in the large-grained inner and outer shells is steep.

The microstructure is established by the reaction heat treatment, and determines the critical current. The best combination of grain size, composition, and volume of the fine-grained shell is obtained with an intermediate reaction temperature (700 to 730°C); this temperature range also yields the best values of J_c. Various two-step heat treatments were studied and compared to isothermal aging. The best microstructure and, hence, the best critical current characteristic was obtained by aging the specimen at 700°C for 4 days followed by 730°C for 2 days.

The onset transition temperature and the transition width were measured inductively. The inductive signal is apparently determined by the properties of the smallest volume of superconducting phase that is sufficient to expel the external magnetic flux. The composition gradient within this volume is then reflected in the transition width. The critical temperature first increased (to ~18K) and then decreased with increasing reaction time.

The J_c characteristic of the multifilamentary wire is compared to that found in preliminary tests on an 'internal tin' bronze-processed wire fabricated by Intermagnetics General. The internal tin wire appears to have a much better critical current density at lower field. Possible metallurgical sources of the higher current density are discussed.

ACKNOWLEDGMENT

This research was supported by the Director, Office of Energy Research, and by the Director, Office of Basic Energy Science, Materials Science Division, and by the Director, Office of High Energy Physics, US Department of Energy under contract number DE-AC03-76SF00098.

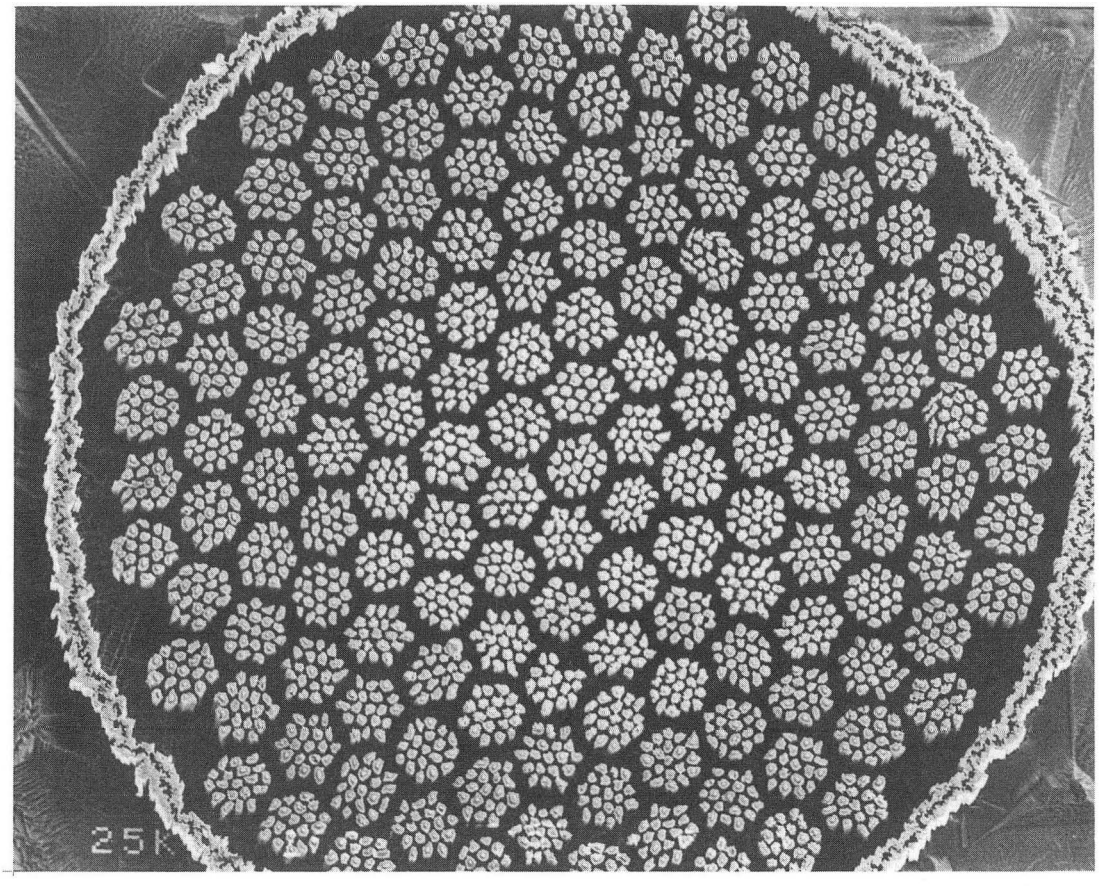

Figure 1. A scanning electron micrograph of a typical reacted bronze-processed multifilamentary wire. Notice that the Ta diffusion barrier constrains the volume expansion of the active core during the diffusion reaction, hence, the Nb_3Sn diffusion layer experiences a radial compressive strain. Without this restrictive layer, the bronze matrix would be able to expand freely and not exert as much stress on the Nb_3Sn layer.

XBB 831-544

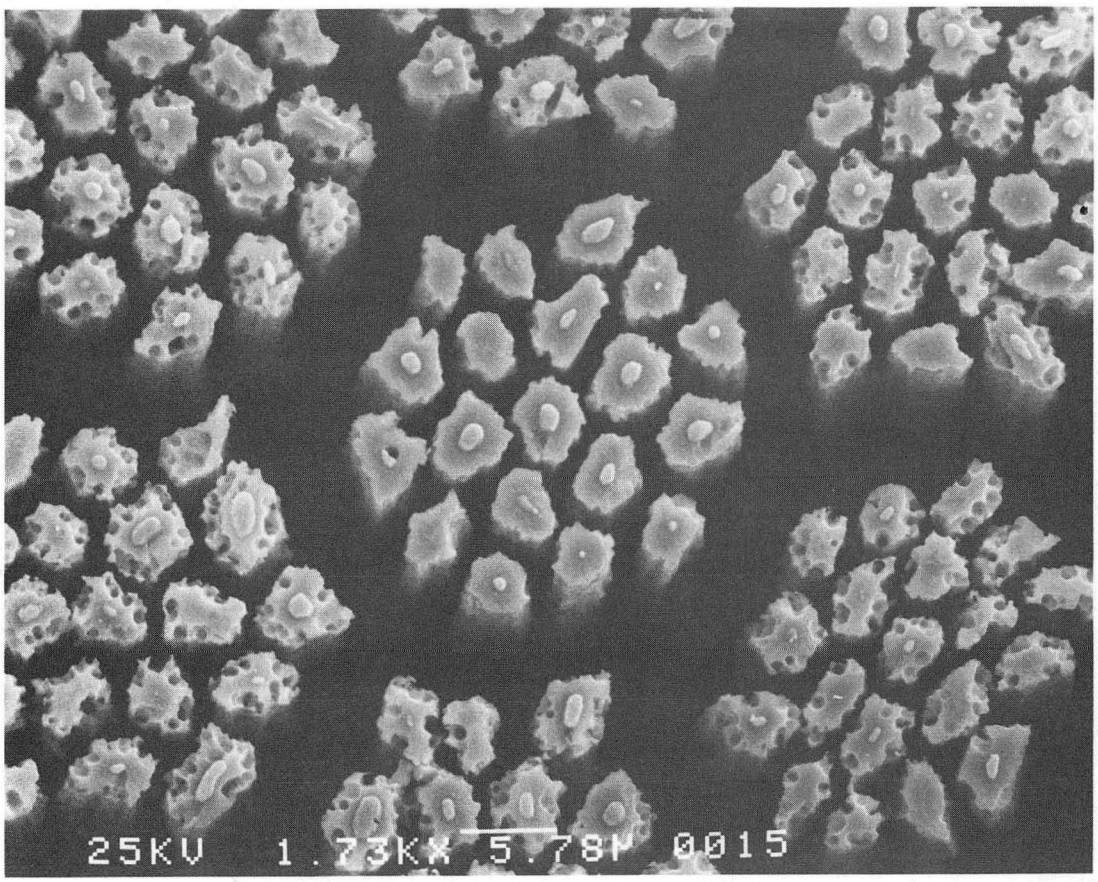

Figure 2. A scanning electron micrograph showing the Nb_3Sn layer and the residual Nb filaments after the bronze matrix has been removed. Voids in the A15 layers, predominately at the periphery of the filaments, are believed to arise from the preferential etching of the A15 grain boundaries due to their high copper concentration.

XBB 831-545

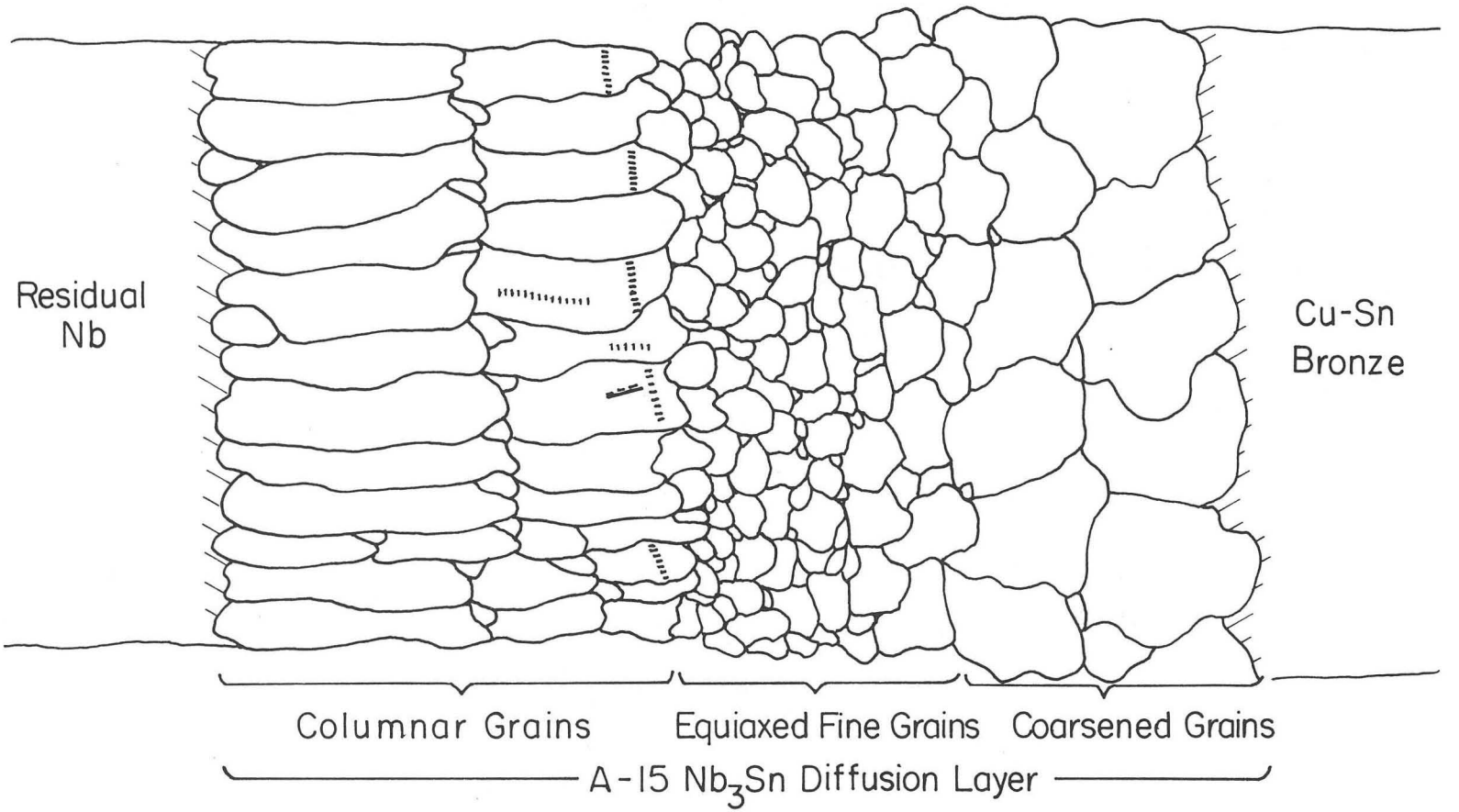

XBL 824-5549

Figure 3. Schematic representation of the grain morphology of the A15 diffusion layer. The direction of the reaction is inward to the Nb filament. As a consequence, a successive layer formation followed the order: columnar grains, fine equiaxed grains and coarsened grains. The transformation of columnar grains to the fine grains is due to the polygonization of dislocation walls to reduce the strain energy associated with the Nb_3Sn layer formation.

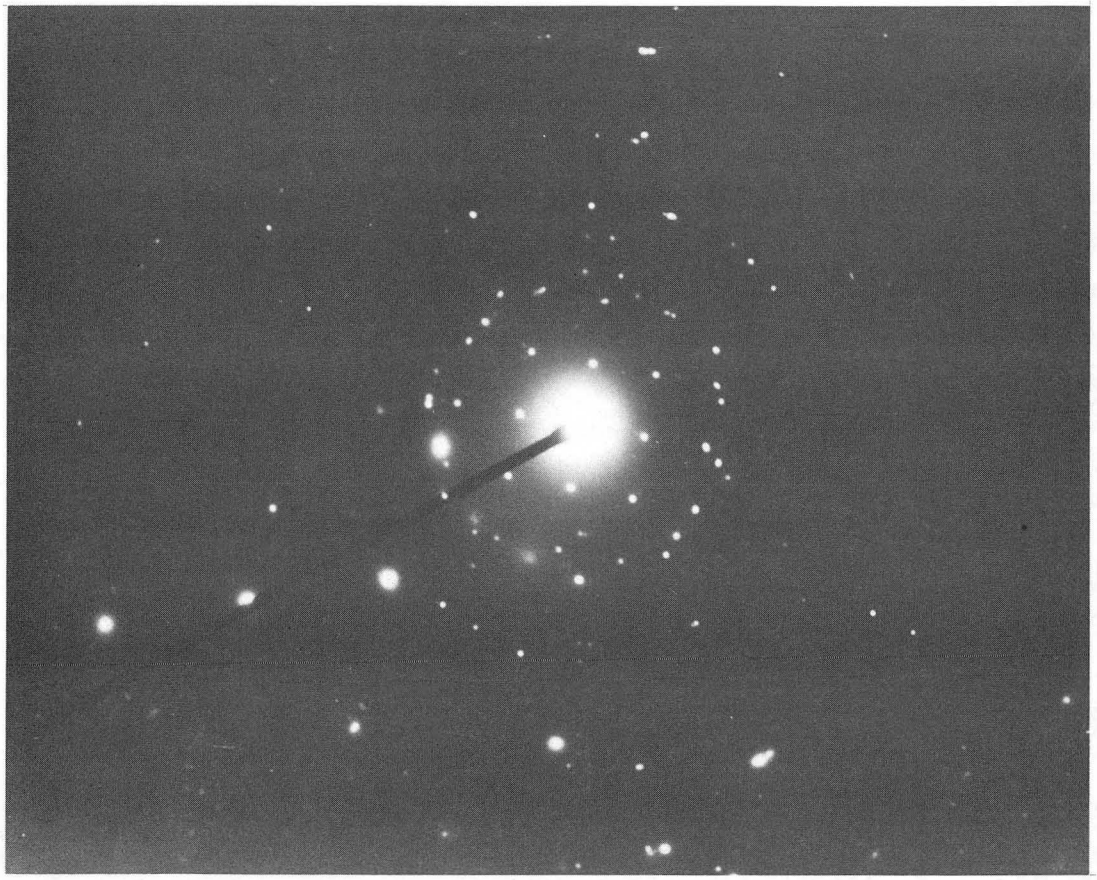

Figure 4. The selected area electron diffraction pattern of the boundary region between the A15 and the residual Nb. The square pattern near the center maximum is the (001) A15 zone axis pattern and the BCC (111) is represented by the brightest diffraction spots.

XBB 822-1159

Figure 5. The corresponding bright field micrograph of Fig. 4 showing the columnar nature of the A15 grains near the Nb interface.

XBB 818-7140

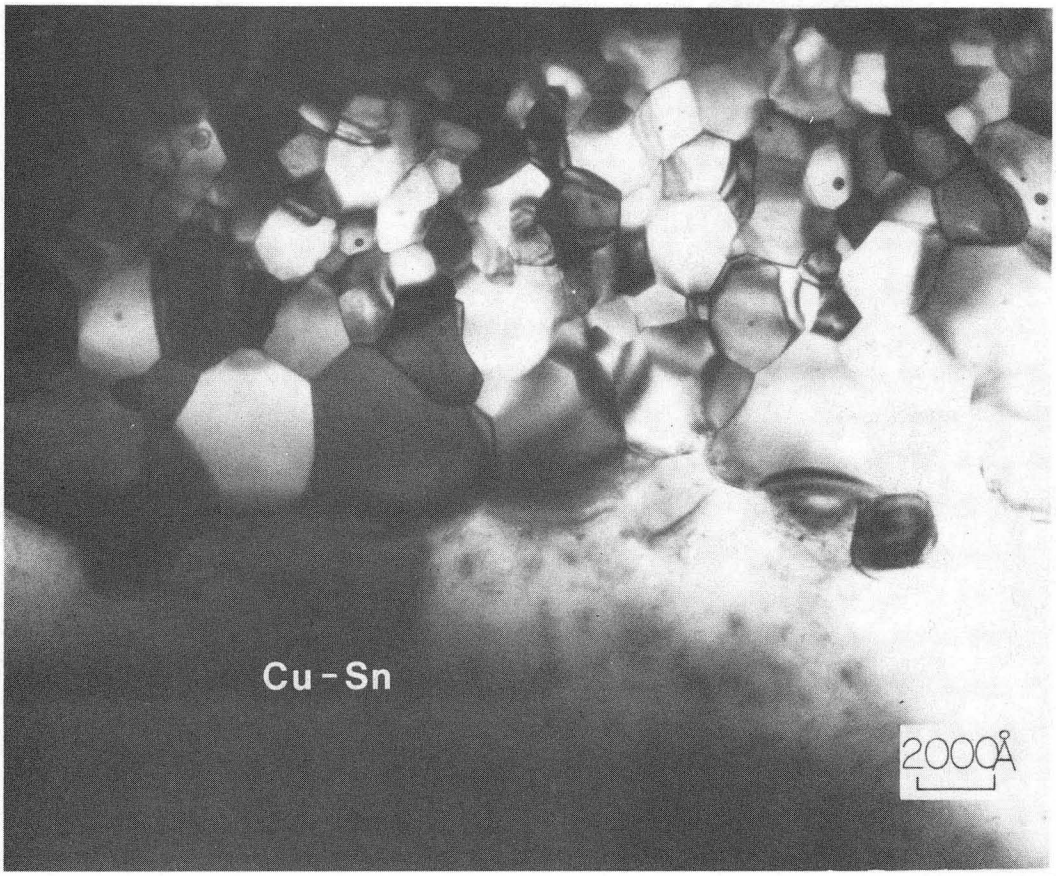

Figure 6. A TEM micrograph showing a typical Nb_3Sn grain morphology near the Nb_3Sn- bronze interface. The coarsened large-grain layer can be seen at the periphery of the reacted filament with the fine equiaxed grain layer adjacent to it.

XBB 824-4088

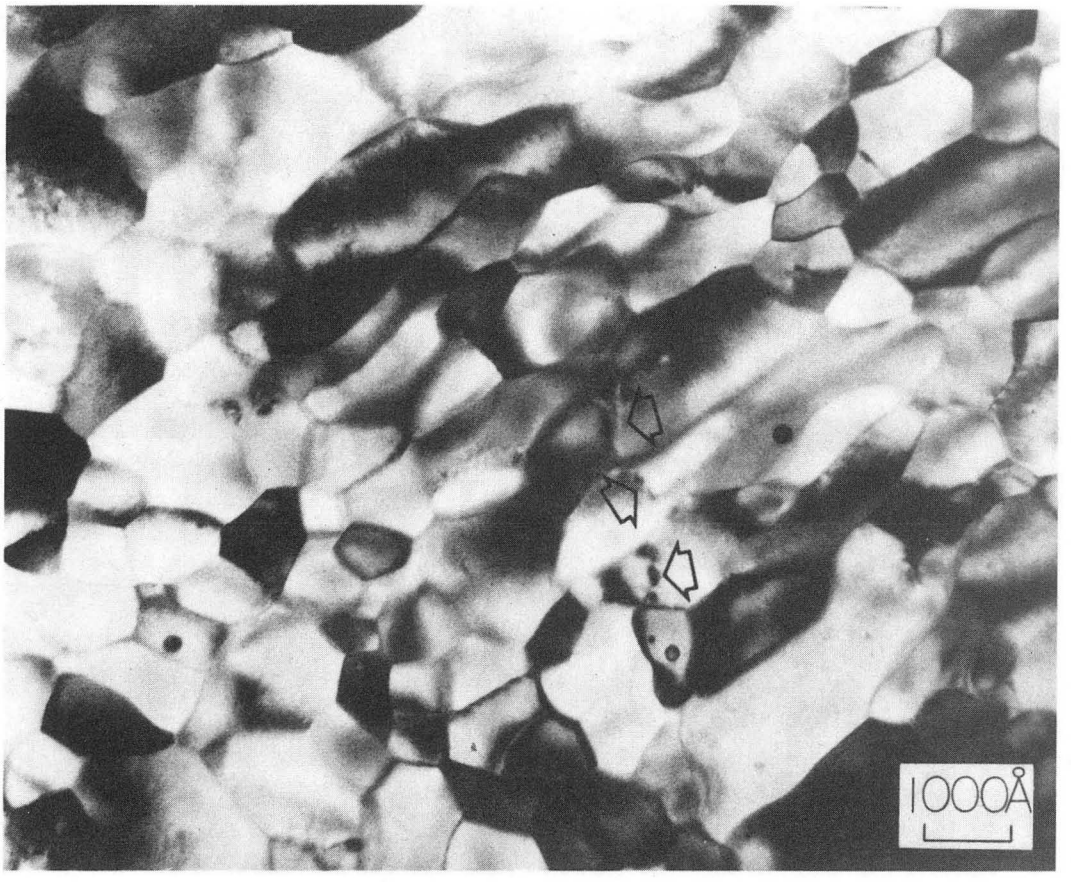

Figure 7. A TEM micrograph revealing the nature of the low angle boundaries between fine equiaxed grains along the direction of elongation of the columnar grains. The columnar grains are to the upper right of the micrograph. Several low-angle grain boundaries are indicated by arrows.

XBB 824-4087

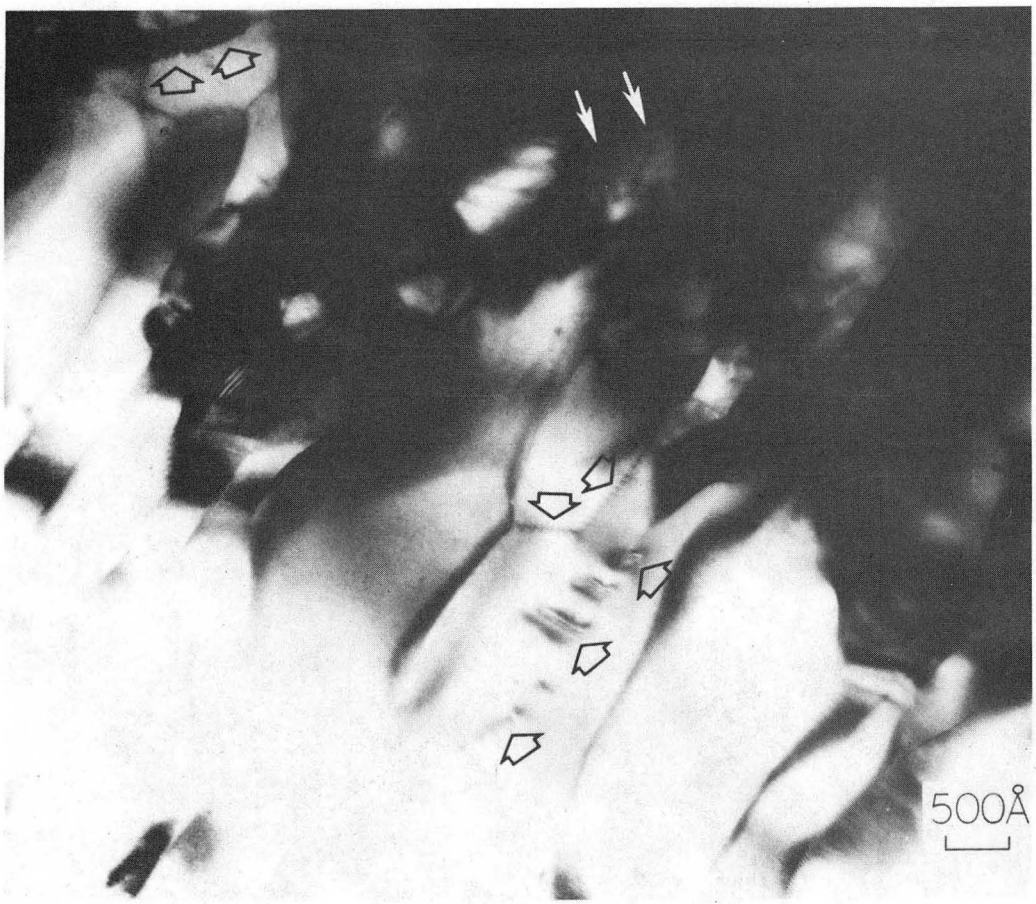

Figure 8. A high resolution TEM micrograph showing dislocation walls in the columnar grains near the Nb interface. Several distinctive dislocation walls are indicated by arrows. The driving force of the dislocations' multiplication and polygonization is believed to be the reduction of the transformation strain energy.

XBB 824-4086

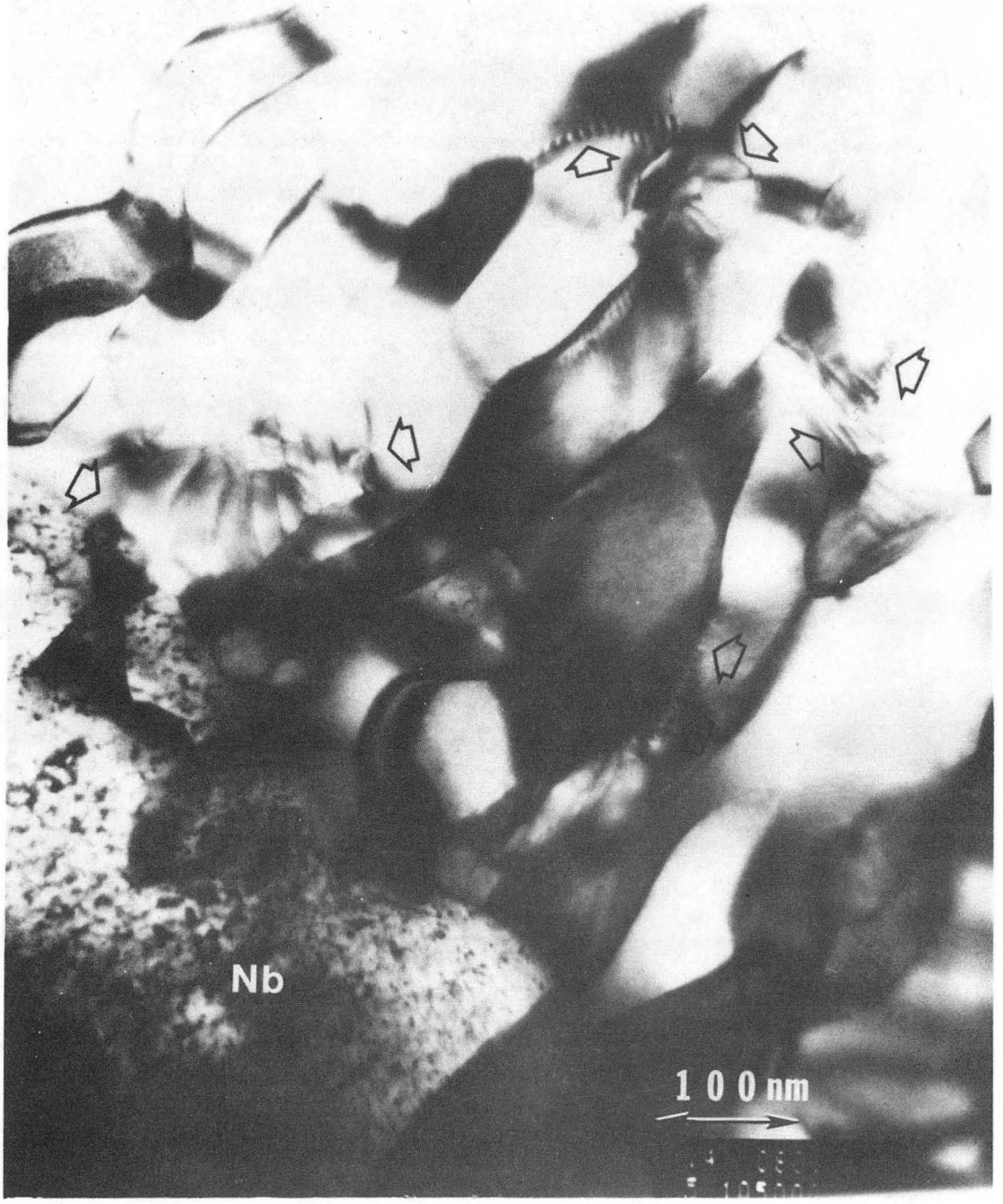

Figure 9. Another high resolution TEM micrograph showing the dislocation walls in the columnar grains near the Nb interface. Notice in the upper right corner of the micrograph that some dislocations polygonized into subgrains while some others are still in the process of polygonization.

XBB 825-4151

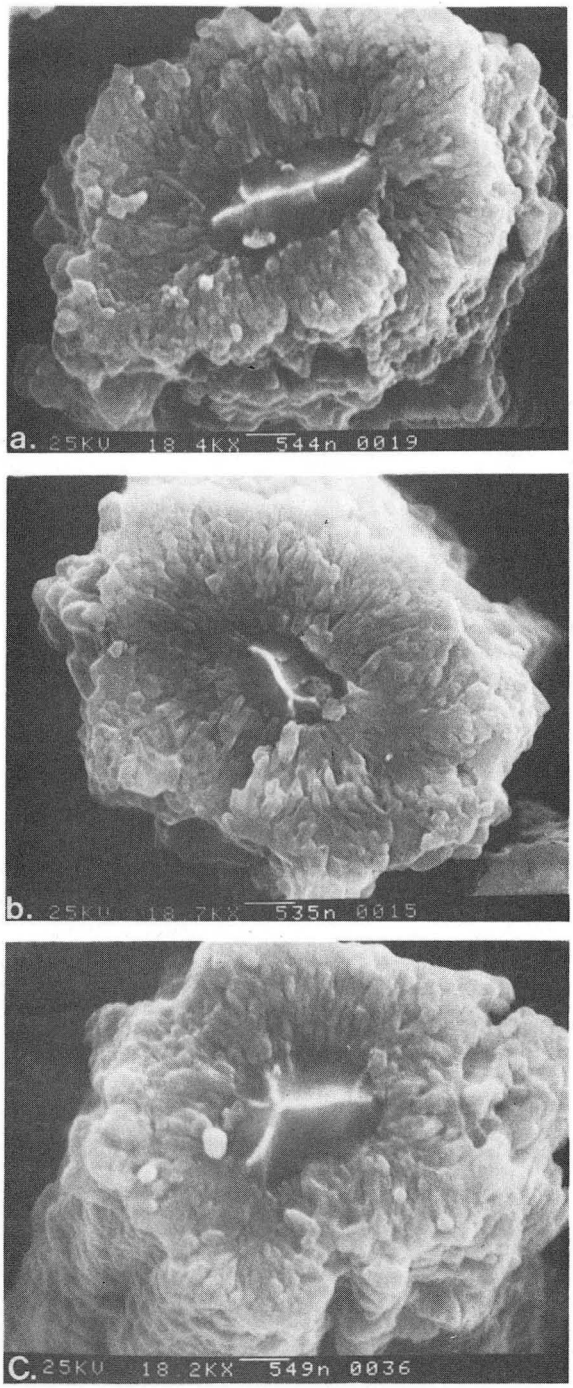

Figure 10. Scanning electron micrographs of the fracture surface of individual filaments heat treated to near 90% reaction at different temperatures. The apparent grain boundaries can be distinguished by the predominate intergranular fracture mode. Lower temperature aging produces a finer grain size. However, the equiaxed grain boundaries are not revealed on the fracture surface due to the nature of the low-angle boundaries. Therefore, to accurately determine the grain size, transmission electron microscopy is required.

XBB 831-229A

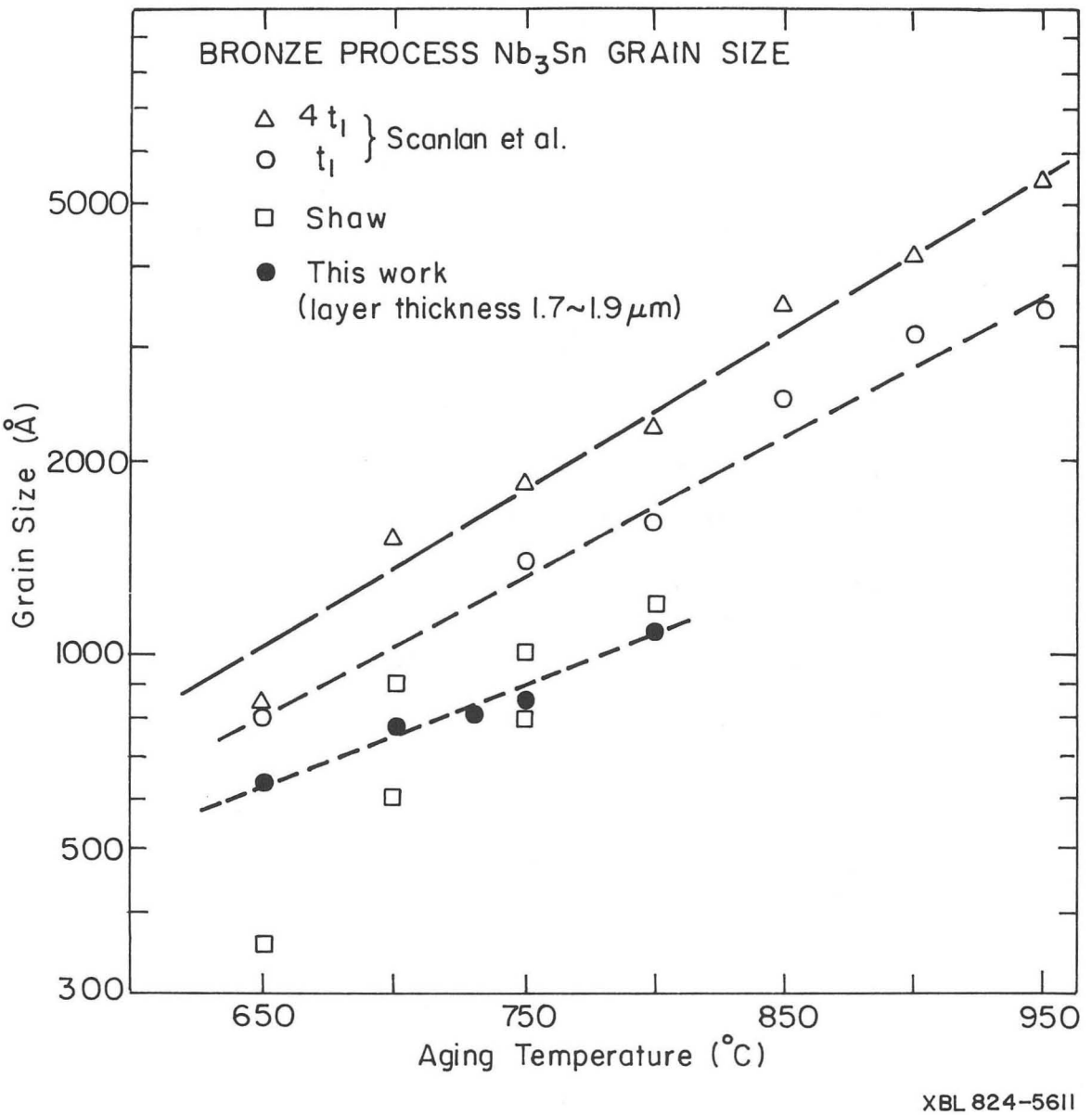

Figure 11. The results of grain size versus aging temperature (650° to 800°C) as determined by a TEM study. The specific data shown in this figure are from the samples heat treated up to the time required to yield a layer thickness ranging from 1.7 to 1.9 ;m. Two other data in the literature on grain size are also included for comparison. It can be concluded that the grain size increases with increasing aging temperature and time, and decreases with decreasing filament diameters.

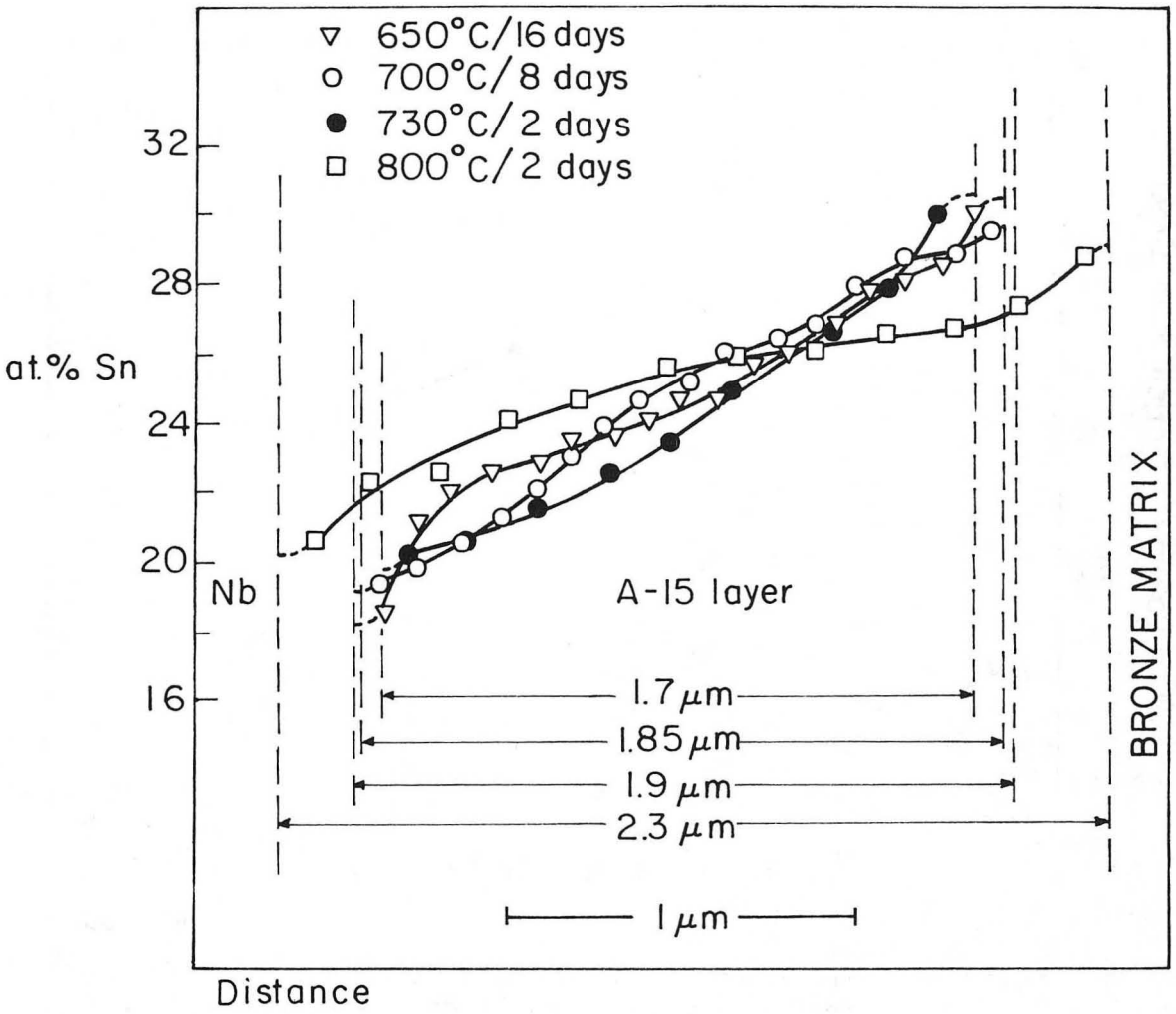

XBL 831-5054

Figure 12. Tin concentration profiles determined by STEM/EDXS analysis across the reacted A15 layer for samples aged to near 90% reaction at various temperatures. The tin concentration decreases monotonically through the layer from a Sn-rich composition at the bronze interface to a Sn-poor composition at the Nb interface. The central region of the A15 layer, where the grain size is small and equiaxial, has a composition close to stoichiometry. The general trend is for the tin concentration gradient to decrease with increasing aging temperature and time.

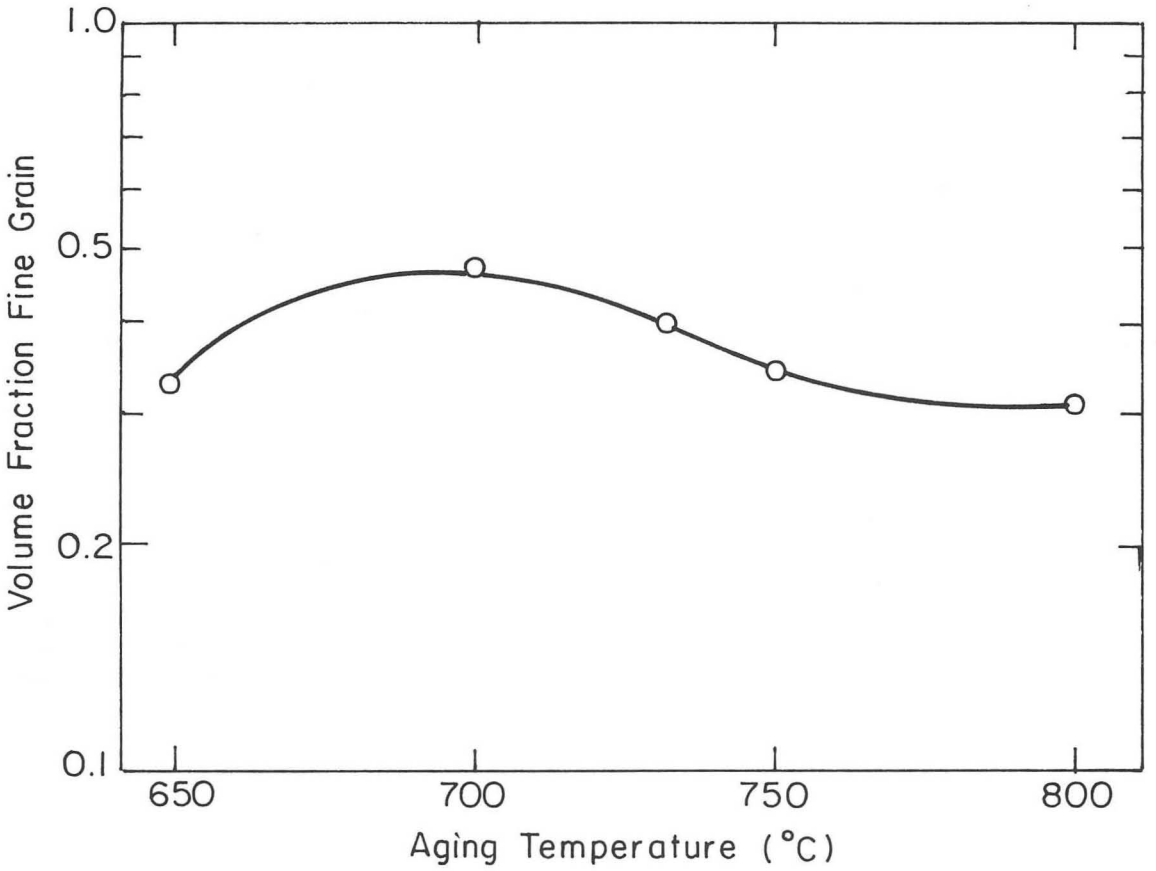

XBL 825-5641

Figure 13. The volume fraction of the fine-grain layer with respect to the original Nb volume versus aging temperature for samples near full reaction. Since this layer contains high density grain boundaries and a near stoichiometric composition, it is the volume that carries the majority of the current near J_c. Two competing factors determine the volume of the fine-grain layer: the mobility of dislocations to polygonize and grain coarsening. Therefore, an optimum temperature (from 700 to 730°C) produces the maximum fine-grain volume.

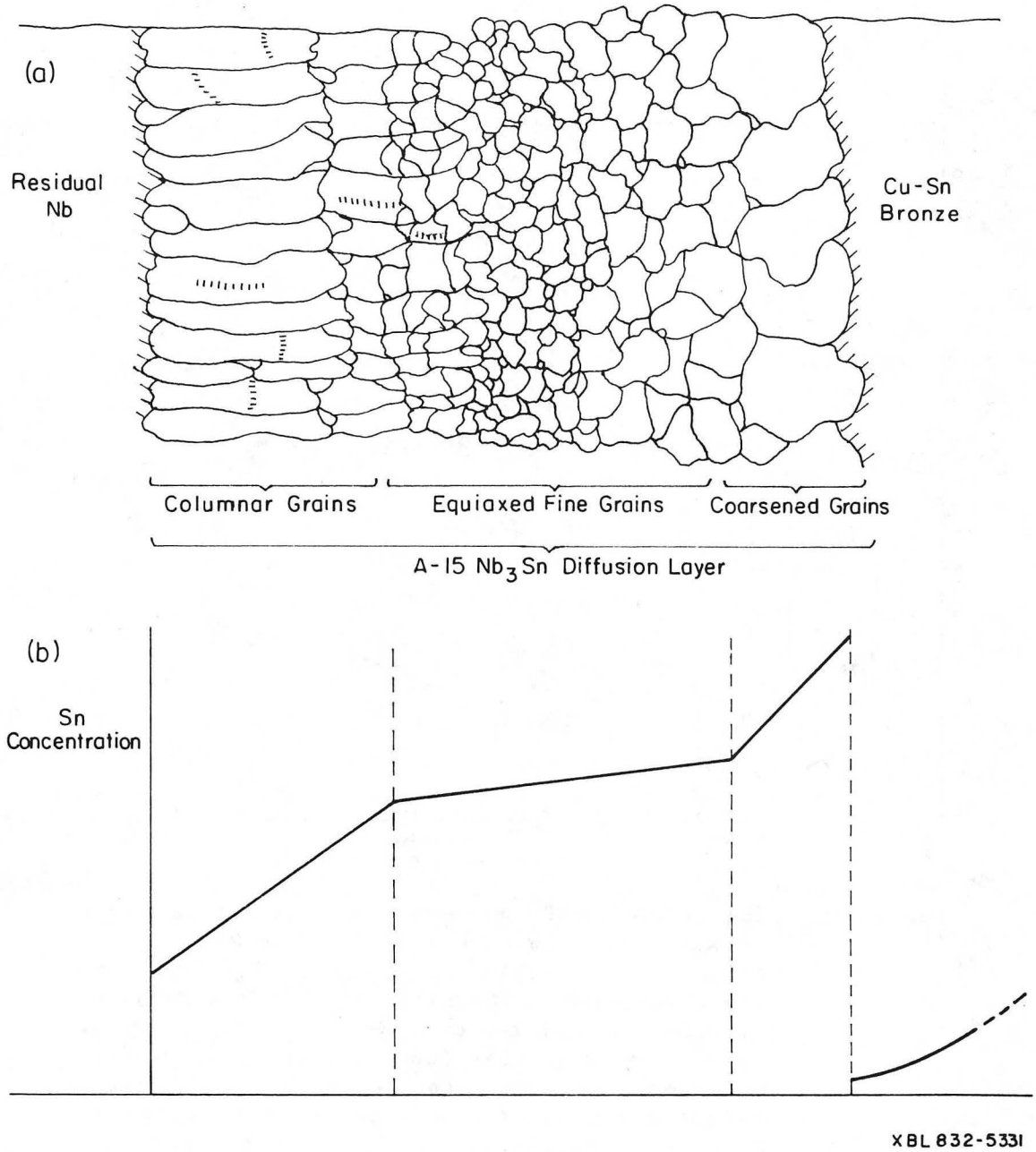

Figure 14. A schematic representation of (a) the grain structure and (b) the tin concentration profile across the A15 layer. It is believed that the flat concentration profile in the fine-grain layer is due to the fast distribution of tin along the grain boundaries.

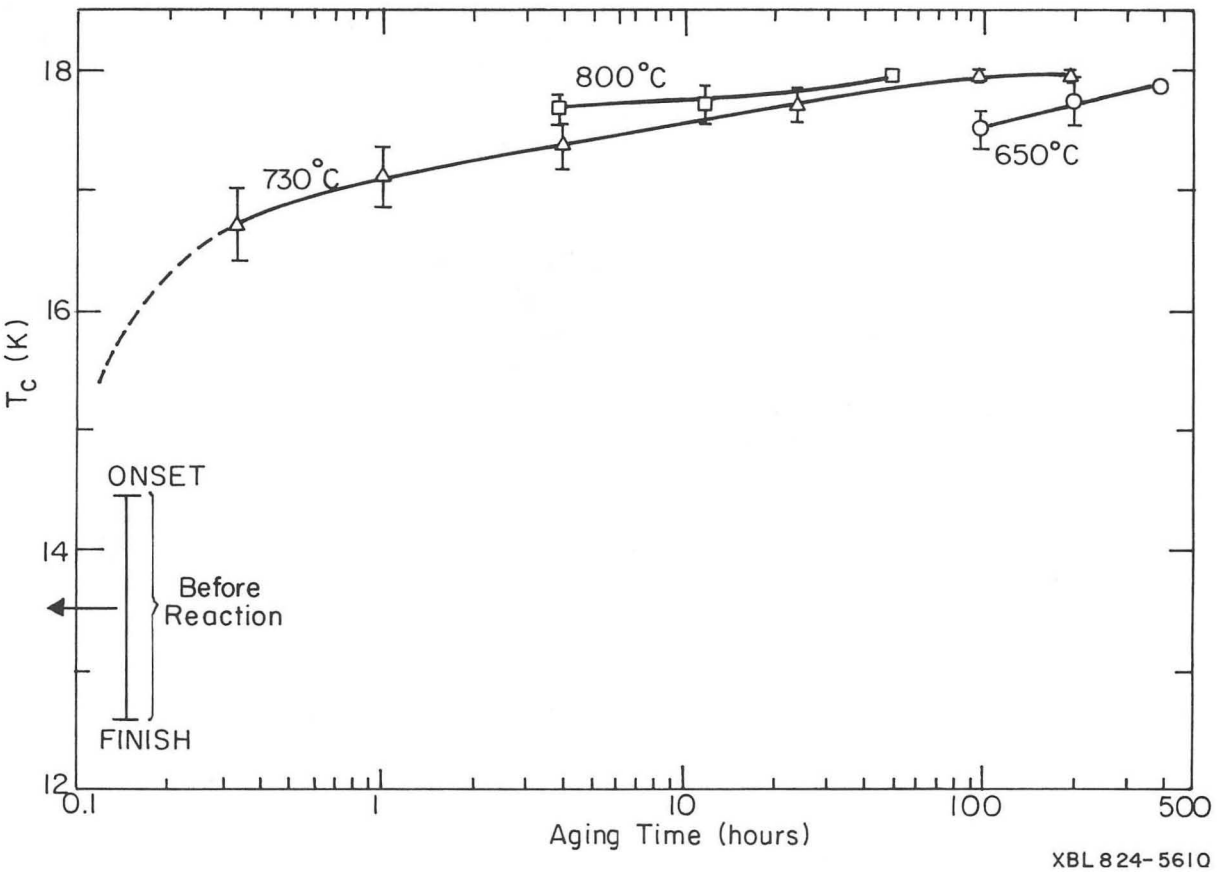

Figure 15. The inductive T_c midpoint and transition width versus aging time for 650, 730 and 800°C. The T_c midpoint increases (to near 18K) and its width decreases with aging time. This behavior is quite general for bronze-processed wires. It can be concluded that the inductive measurement, which measures the change in slope of M-H curve within the field range of the applied oscillating field amplitude, yields only the information about the volume of superconducting phase enough to expel the external flux. In our measurement, this volume is estimated to be ~1 μm in layer thickness.

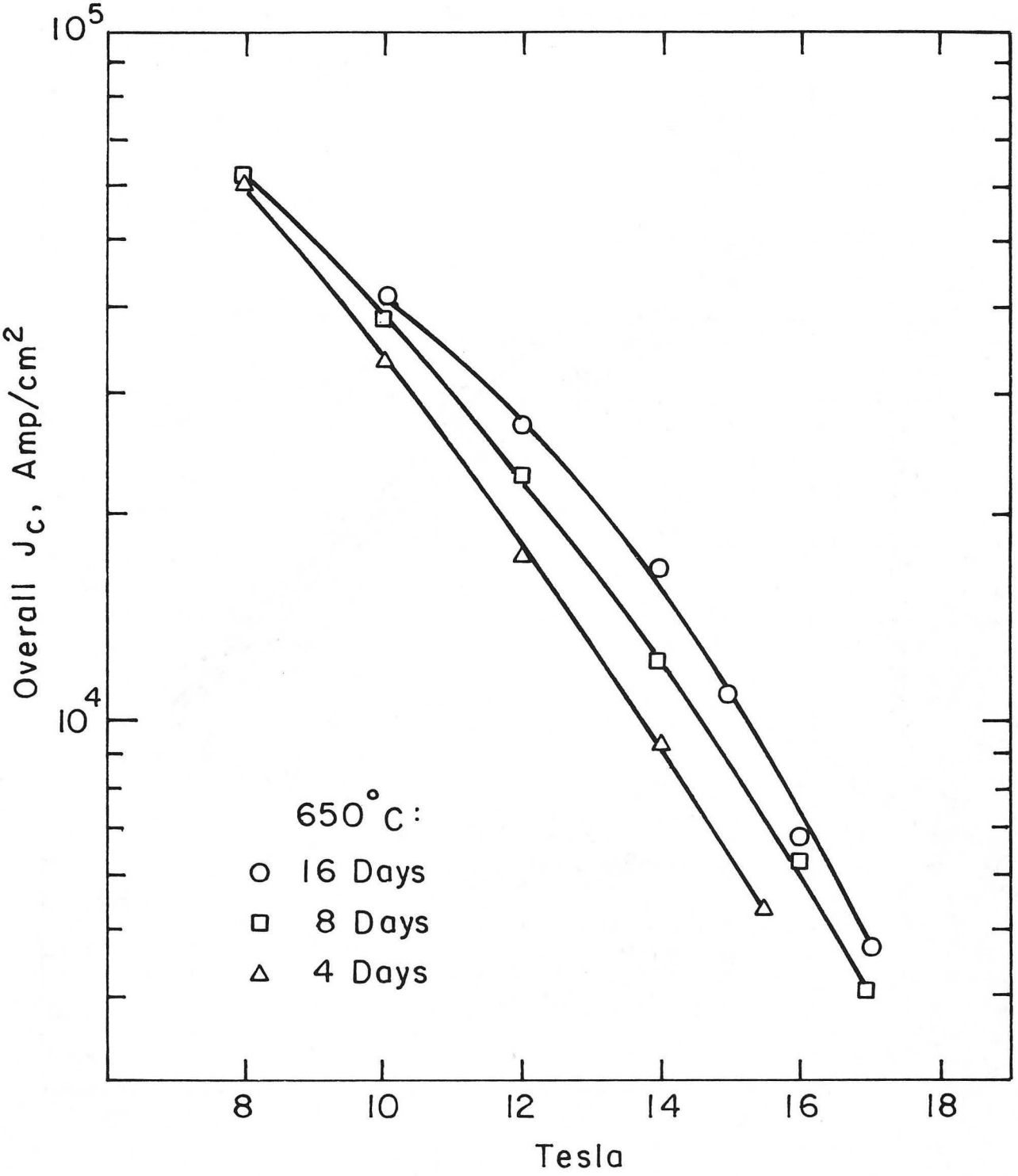

XBL 822-5156

Figure 16. The $J_c(H)$ characteristics of samples aged at 650°C. Microstructural studies revealed that the fine grain size for short heat treatments are responsible for the high J_c at lower fields even though the volume of the fine grain layer is smaller and has a higher concentration gradient. Prolonging the aging time to 16 days mainly increases J_c at higher fields.

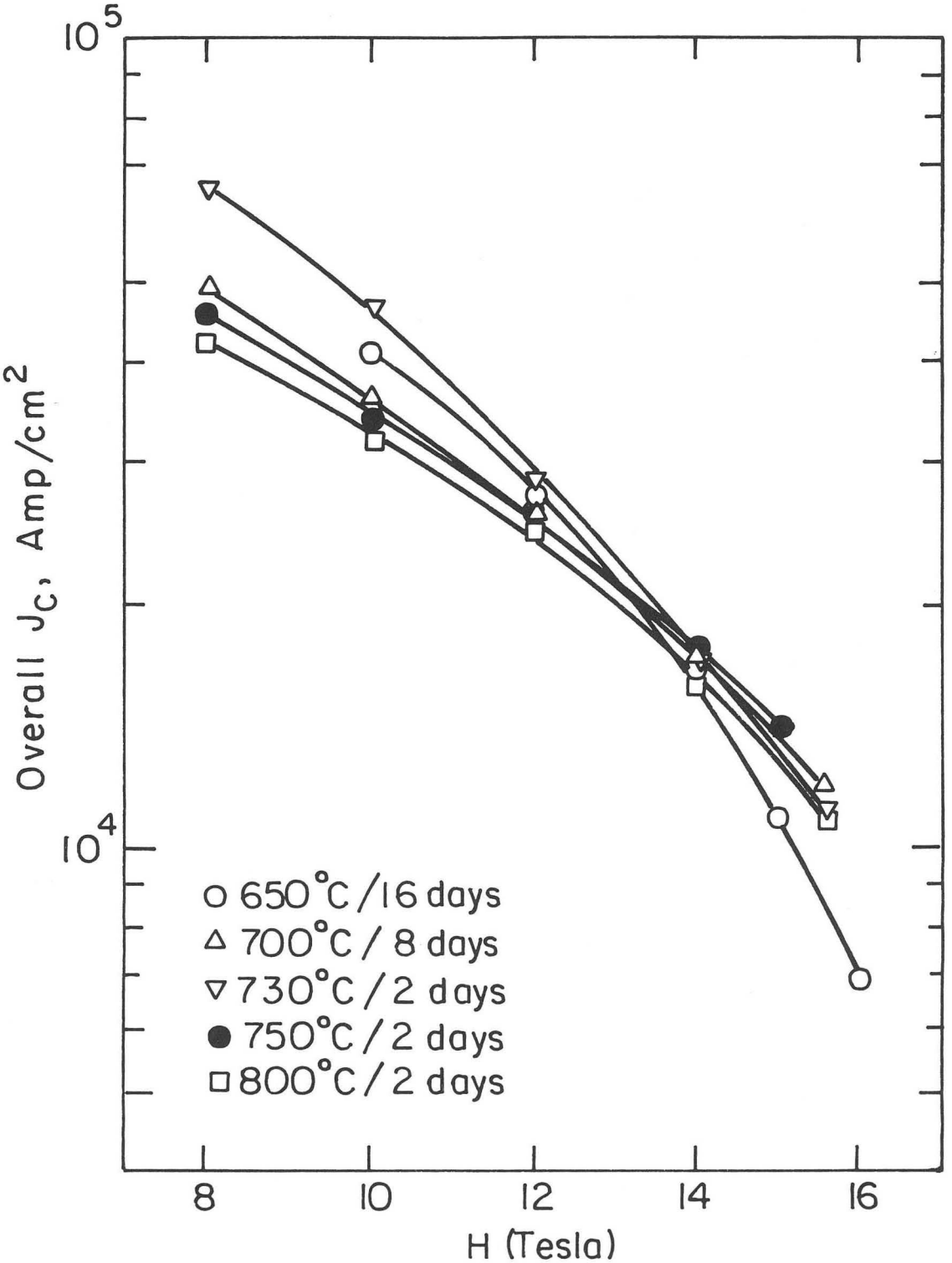

Figure 17. The $J_c(H)$ characteristics of samples heat treated in the temperature range 700 to 800 °C. Heat treatments at intermediate temperature and time give the best $J_c(H)$ characteristics. For example, samples aged at 700°C for 6 days and 730°C for 2 days show the best J_c at all fields.

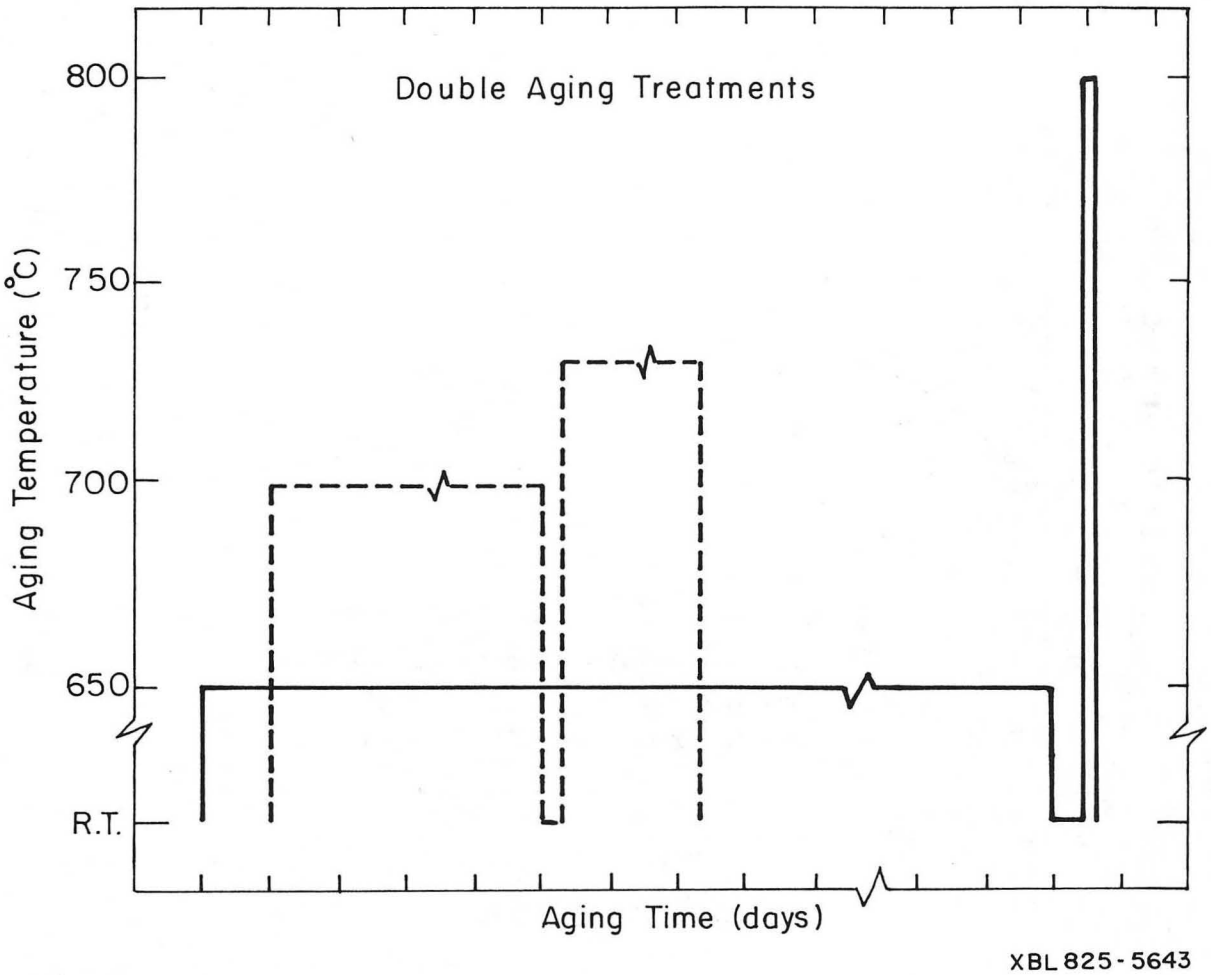

Figure 18. Schematic heat treatment schedules to improve the microstructural state of A15 layers. The first-stage heat treatment is at a low temperature to establish a fine-grain structure and the second-stage heat treatment at higher temperature is designed to redistribute the tin within the fine-grained layer. The necessary condition for this modified heat treatment to work is that the redistribution of tin be a faster process than the Nb_3Sn grain coarsening introduced by the second-stage higher temperature treatment.

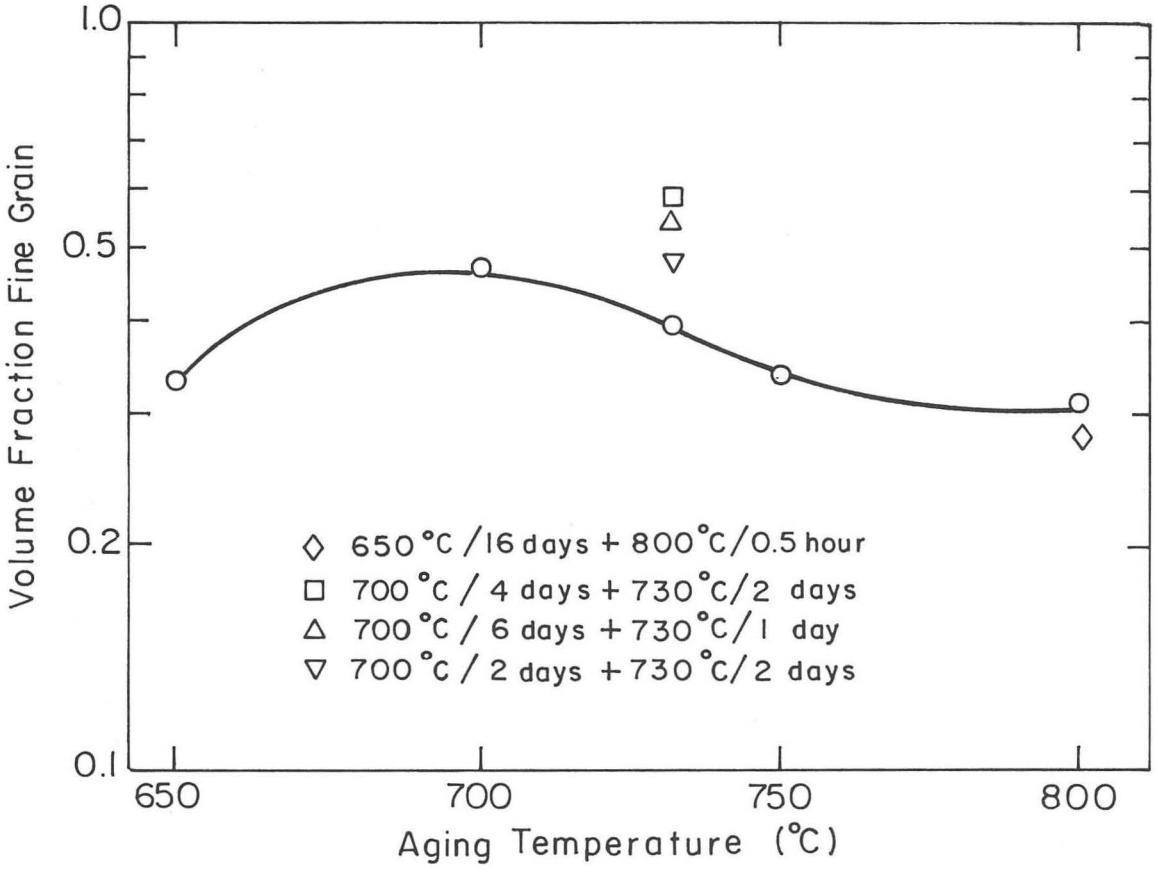

XBL 825-5642

Figure 19. The volume fraction of the fine grain layer for several double-aged specimens as compared with that of the isothermally prepared samples. The samples aged at 700°C and then followed by 730°C show an increase in the volume fraction, while the 650°C + 800°C heat treatment produces a lower fraction. This can be attributed to the increase in the dislocation mobility without significant coarsening at the 730°C treatment.

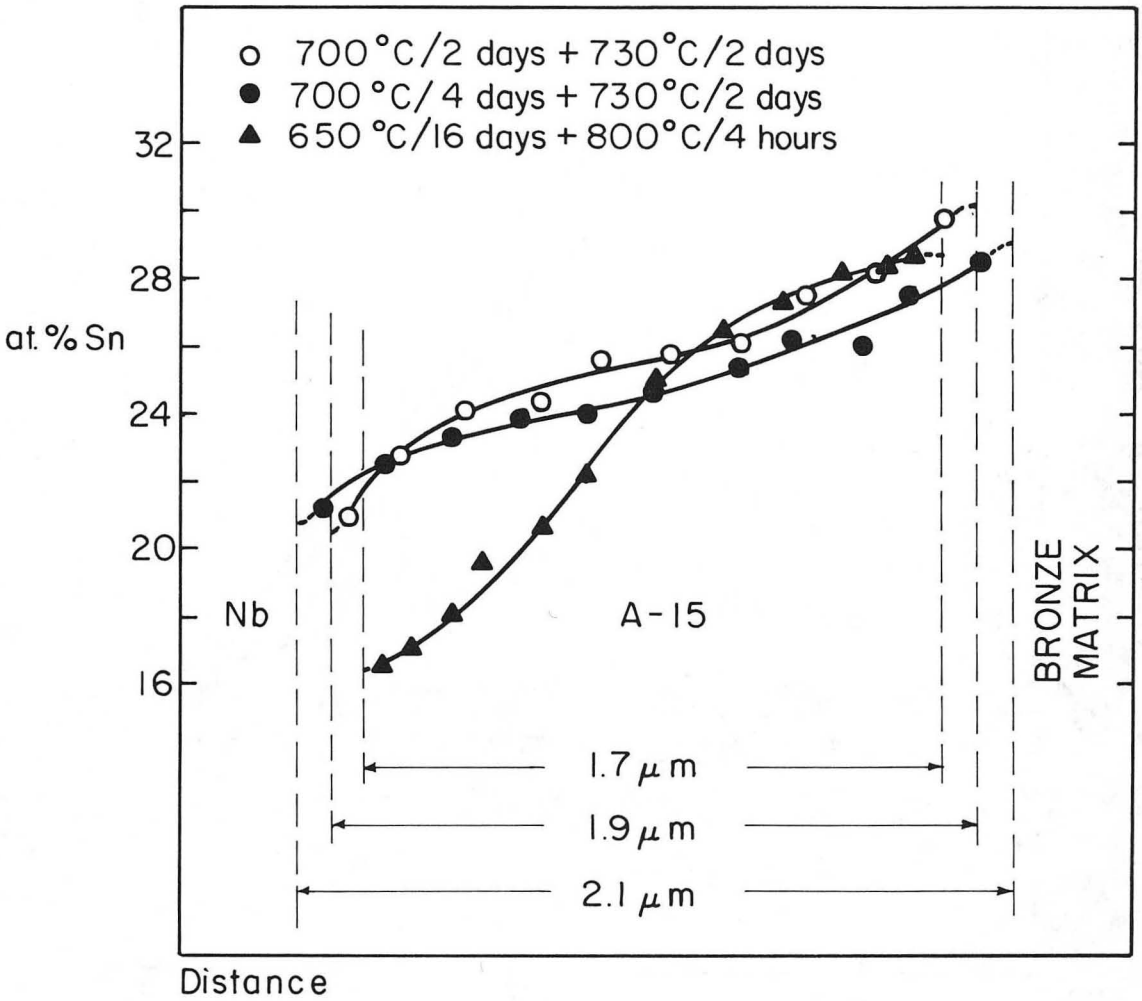

XBL 817-6193

Figure 20. The STEM/EDXS analysis of the tin concentration profiles of three double-aged specimens. The small composition gradient of the 700 + 730°C aged specimens shown in this figure is favorable, while the steep gradient of the sample treated at 650°C for 16 days + 800°C for 4 hours is undesirable and yields inferior J_c.

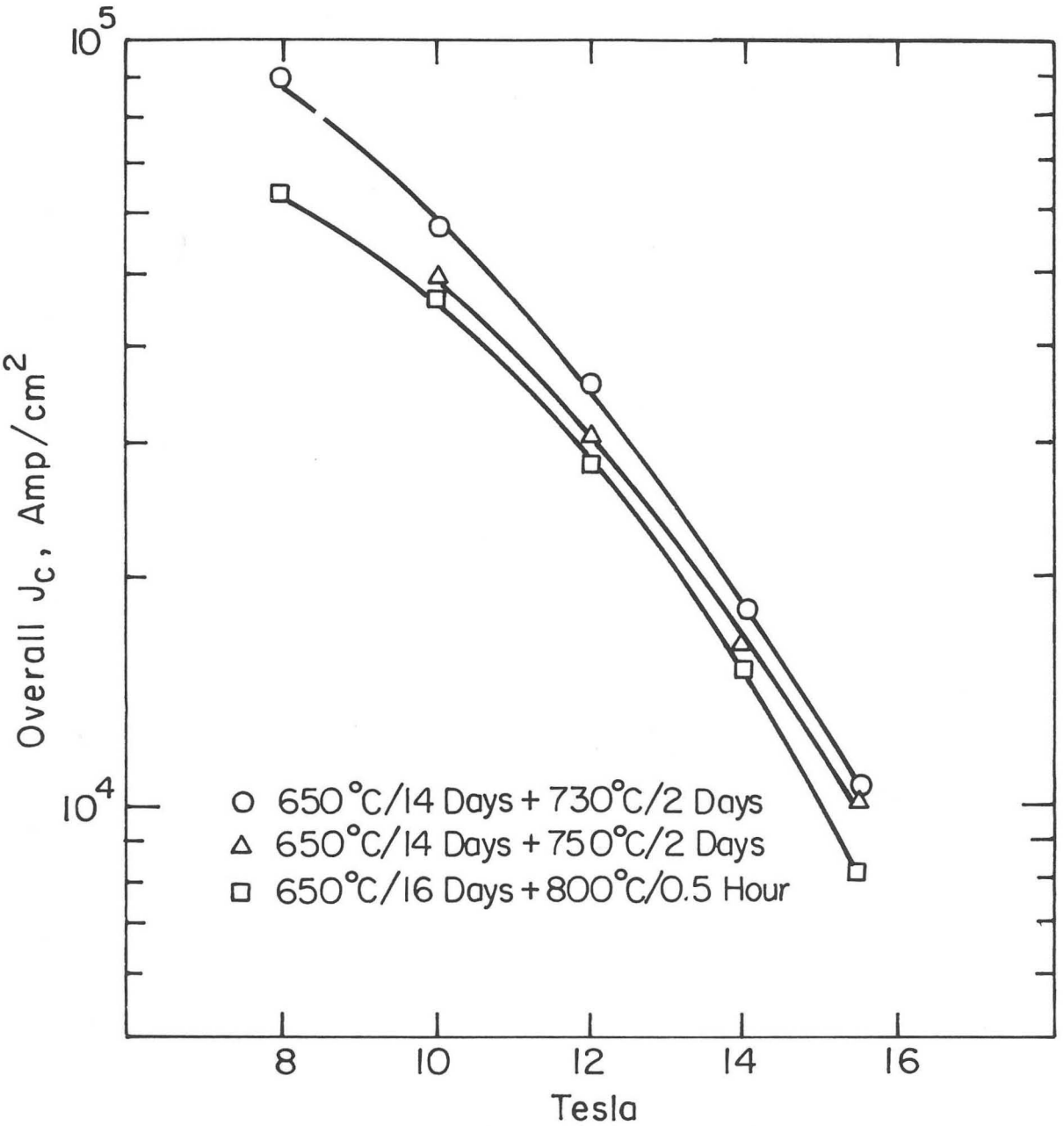

Figure 21. The $J_c(H)$ characteristics of double-aged specimens starting with 650°C and followed by various higher temperature treatments. From the data it is clear that the higher the second aging temperature, the smaller the J_c enhancement.

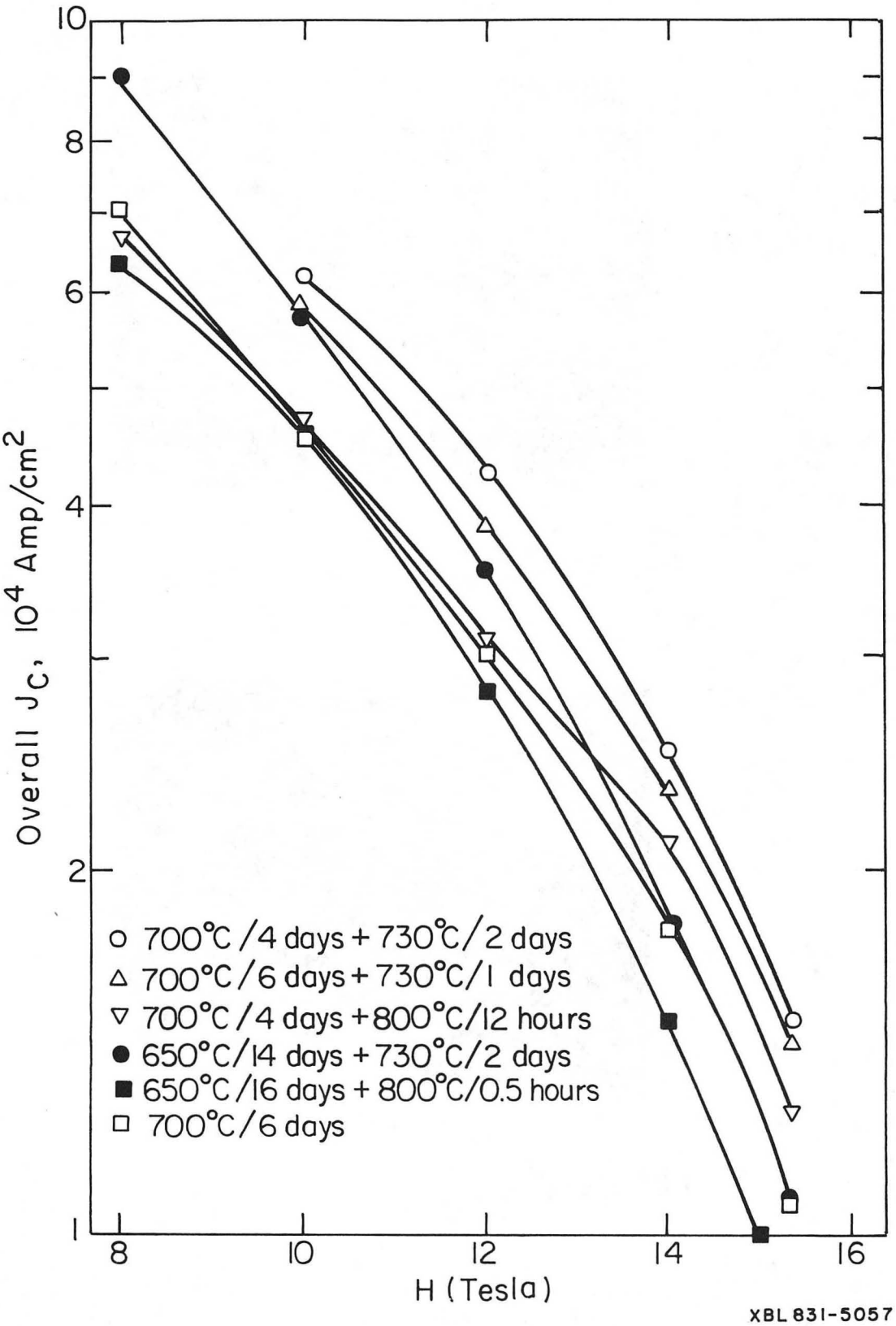

Figure 22. The $J_c(H)$ characteristics of several double-aged samples with 700°C as the starting heat treatment temperature. The $J_c(H)$ of the 700°C/6 days sample is also included, representing the best obtained by isothermal aging. The 700°C/4 days + 730°C/2 days sample has about a 50% increase in the J_c over that of the 700°C/6 days.

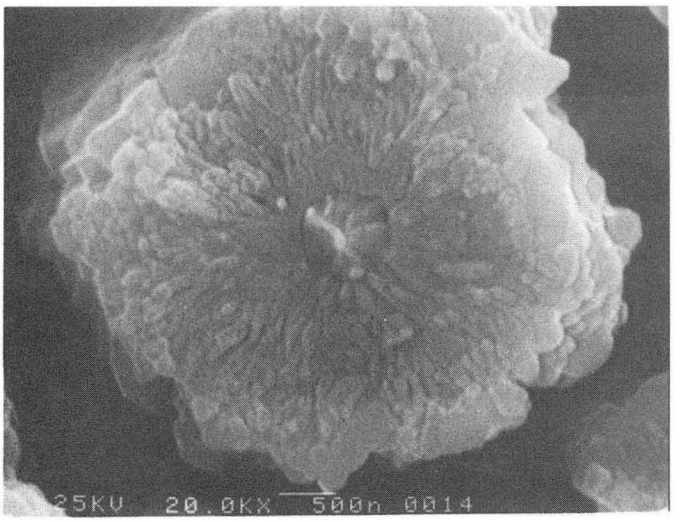

(a) $650^{\circ}C/14D, 730^{\circ}C/2D$

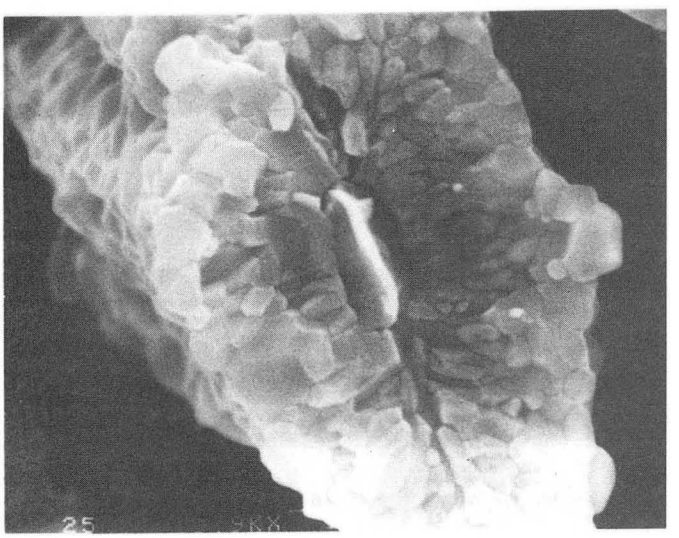

(b) $800^{\circ}C/2D$

Figure 23. The SEM micrographs of the fracture filaments aged at (a) 650°C/14 days + 730°C/2 days, and (b) 800°C/2 days. A significant difference in the apparent grain size with varying heat treatment conditions can be noticed. Also, the intergranular fracture mode of the A15 phase is very distinct (b).

XBB 824-4084

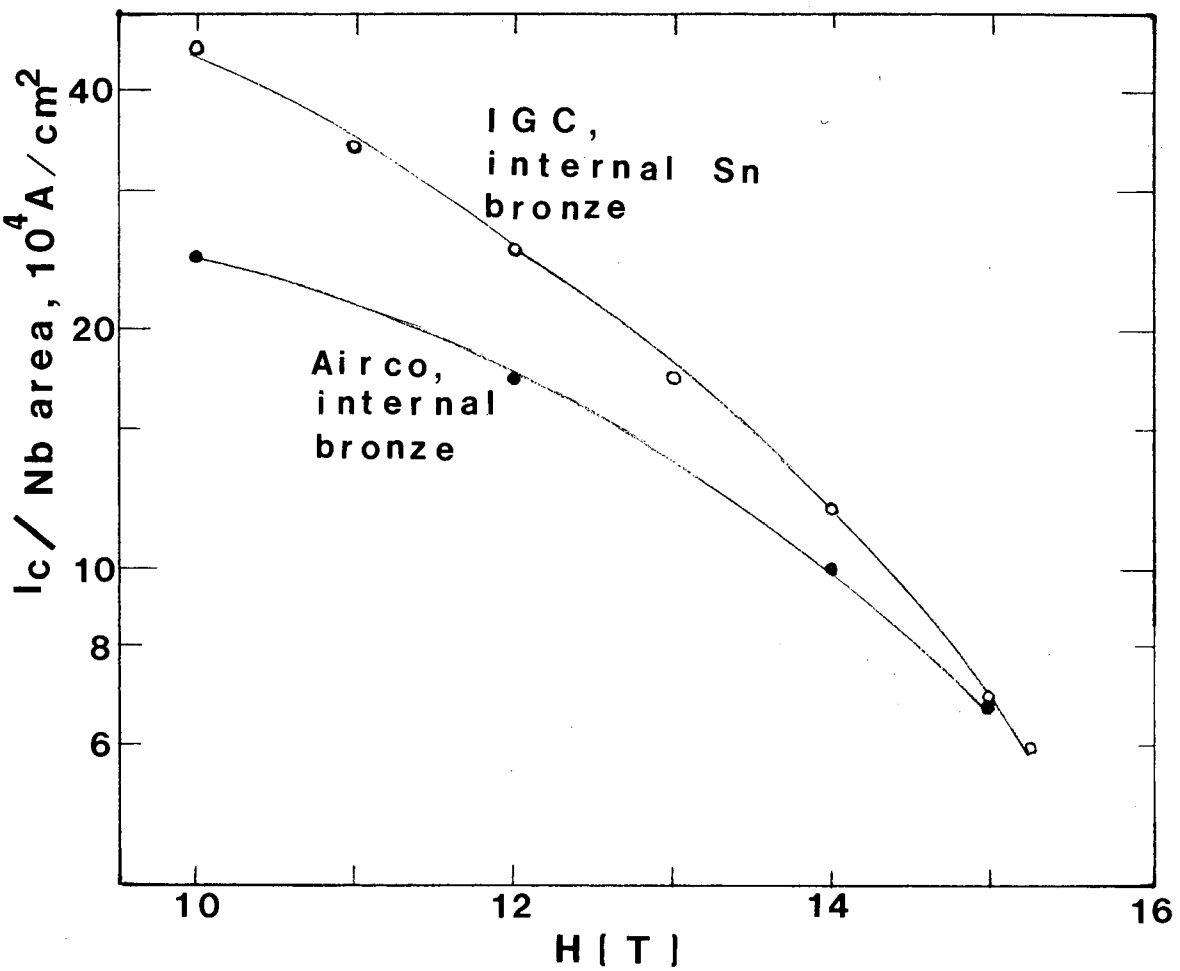

XBL 836-10200

Figure 24. A comparison of $I_c(H)$ divided by the initial Nb area of the 'internal bronze' Airco wire and the 'internal tin bronze' IGC wire. The Airco wire data in this figure is the best obtained by double-aging treatment. The IGC sample cited in this figure represents the best heat treatment condition of a recent preliminary study. By optimizing the heat treatment, it is expected that this value can be improved further. A significant increase in J_c, especially in the lower field range, is clear. The improvement is most likely due to the microstructural sources introduced by the change of diffusion condition.

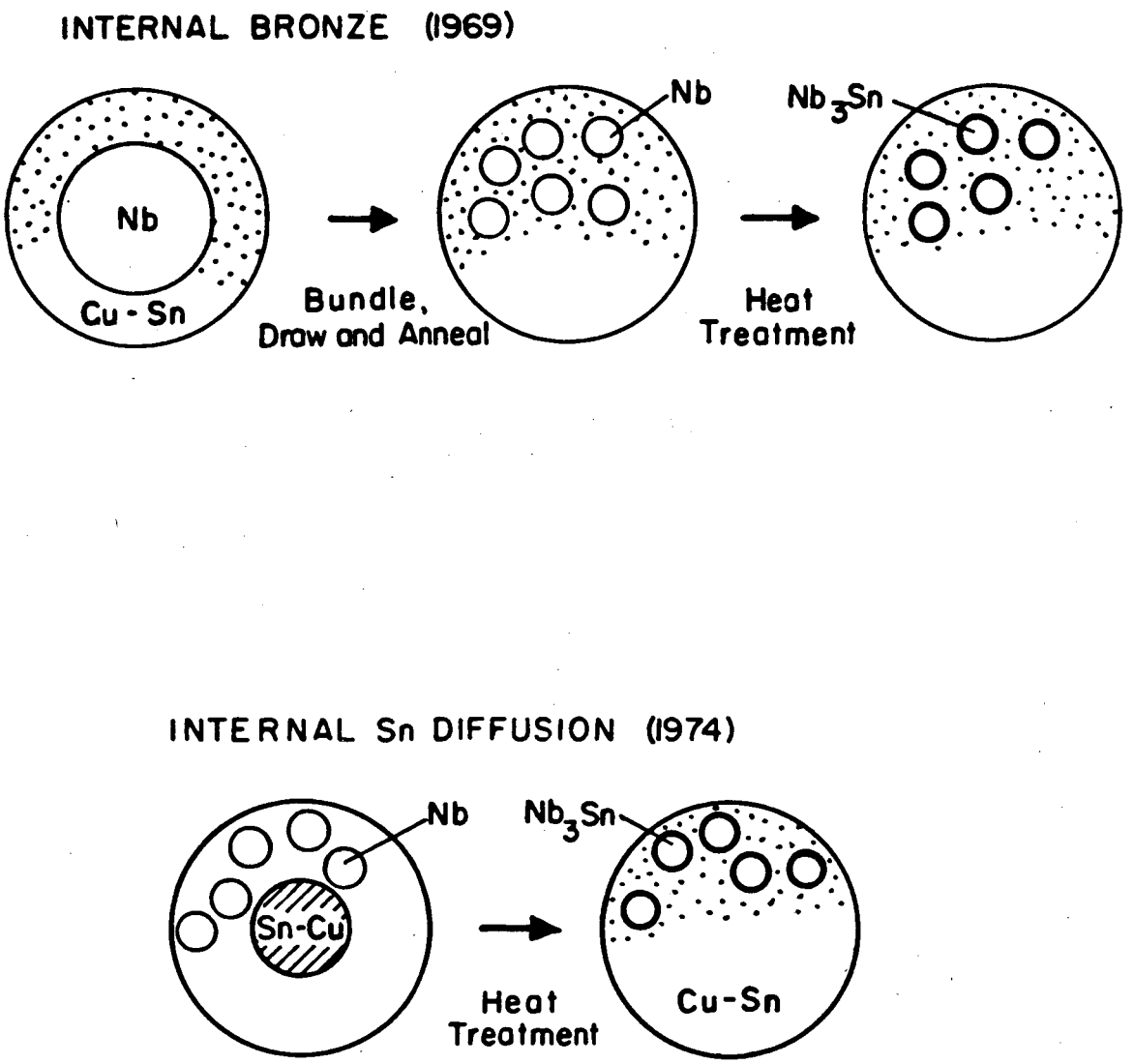

XBL 836-10199

Figure 25. Schematic rep resentations of the 'internal bronze' and the 'internal tin bronze' processes for the multifilamentary Nb_3Sn wire. It can be recognized that the main difference between these two processes is that the 'internal tin bronze' process has a continuous supply of tin instead of sequential depletion of tin in the bronze matrix. The grain size will be smaller due to a higher nucleation rate. The fact that it is easier to draw the wire down to smaller size encourages finer filaments. The fine filaments will, react thus eliminating the low tin con centration boundary at the Nb interface. As a result, a larger volume of the A15 phase can be closer to stoichiometric composition.

TECHNICAL INFORMATION DEPARTMENT
LAWRENCE BERKELEY LABORATORY
UNIVERSITY OF CALIFORNIA
BERKELEY, CALIFORNIA 94720